A Superficial Intramolecular Alignment of Carbon Nitride through Conjugated Monomer for Optimized Photocatalytic CO$_2$ Reduction

Asif Hayat [1,†], Muhammad Sohail [2,†], T.A. Taha [3,4], Asma M. Alenad [5], Ikram Uddin [6], Ashiq Hayat [7], Tariq Ali [8], Rahim Shah [8], Ahmad Irfan [9], Wasim Ullah Khan [10], Arkom Palamanit [11], Yas Al-Hadeethi [12,13], Jawad Ali Shah Syed [14], Mohammed A. Amin [15,*], Javid Khan [16,*] and Sunil Kumar Baburao Mane [17,*]

1   State Key Laboratory of Photocatalysis on Energy and Environment, College of Chemistry, Fuzhou University, Fuzhou 350116, China; asifncp11@yahoo.com
2   Institute for Advanced Study, Shenzhen University, Shenzhen 518060, China; sohailncp@gmail.com
3   Physics Department, College of Science, Jouf University, Sakaka 75471, Saudi Arabia; themaida@ju.edu.sa
4   Physics and Engineering Mathematics Department, Faculty of Electronic Engineering, Menoufia University, Menouf 32952, Egypt
5   Chemistry Department, College of Science, Jouf University, Sakaka 7547, Saudi Arabia; amenad@ju.edu.sa
6   CAS Key Laboratory of Science and Technology on Applied Catalysis, Dalian Institute of Chemical Physics, Chinese Academy of Sciences, Dalian 116023, China; ikram@dicp.ac.cn
7   Department of Physics, Quaid-e-Azam University, Islamabad 45620, Pakistan; ashiqhayath02@gmail.com
8   Soochow Institute for Energy and Materials Innovations, College of Energy, Soochow University, Suzhou 215006, China; norganica@gmail.com (T.A.); Rahimscholar@gmail.com (R.S.)
9   Department of Chemistry, College of Science, King Khalid University, Abha 61413, Saudi Arabia; ahmeed@kku.edu.sa
10 State Key Laboratory of Optoelectronic Materials and Technologies, School of Materials Science and Engineering, Sun Yat-sen University, Guangzhou 510275, China; wasimullah89@yahoo.com
11 Energy Technology Program, Department of Specialized Engineering, Faculty of Engineering, Prince of Songkla University, 15 Karnjanavanich Rd., Songkhla 90110, Thailand; energy_man001@hotmail.com
12 Department of Physics, Faculty of Science, King AbdulAziz University, Jeddah 21589, Saudi Arabia; yalhadeethi@kau.edu.sa
13 Lithography in Devices Fabrication Research Group, Deanship of Scientific Research, King AbdulAziz University, Jeddah 21589, Saudi Arabia
14 Department of Material Science and Engineering, College of Engineering and Applied Sciences, Nanjing University, Nanjing 210023, China; syedjawadalishah89@gmail.com
15 Department of Chemistry, College of Science, Taif University, Taif 21944, Saudi Arabia
16 School of Chemistry, Sun Yat-Sen University, Guangzhou 510275, China
17 Department of Chemistry, Khaja Bandanawaz University, Gulbarga 585101, India
*   Correspondence: Mohamed@tu.edu.sa (M.A.A.); khanj3@mail.sysu.edu.cn (J.K.); mane@mail.sysu.edu.cn (S.K.B.M.); Tel.: +96-6545707507 (M.A.A.); +86-20-84111823 (J.K.); +91-8095027725 (S.K.B.M.)
†   These authors are equally contributed.

Abstract: One of the most frequent ways to widen the adsorption range of carbon nitride (CN) is to add a well-known photosensitizer into its basic structure. So far, such attachments have been accomplished by using weak van der Waals forces. However, using strong covalent bonding to attach such photosensitizer with CN is yet to be determined. Here, for the first time, we covalently bonded porphyrin (5,10,15,20-tetrakis(4-(2,4-diamino-1,3,5-triazinyl) phenyl)-Porphyrin (TDP)), a renowned photosensitizer, effectively with CN by thermally balanced molecular strategy. A photoreaction system was set up for the deoxygenated conversion of CO$_2$ to CO under visible light, where cobalt acted as a redox controller to speed up the charge transportation, while CN-TDP worked as a CO$_2$ activating photocatalyst. The subsequent photocatalyst has a broader absorbance range, a greater specific surface area, and intramolecular organic connections that help to decrease the electron-hole pairs' recombination rate. Furthermore, the average weight ratio between urea and TDP was well-tuned, resulting in a fantastic CO$_2$ photoconversion for CN-TDP$_{7.0}$ compared to the blank sample. This substantial increase in photocatalytic activity predicts a significant shift in CN's specific surface area, band gap, chemical composition, and structure, as well as the efficient separation of

photogenerated charge carriers from the ground state (HOMO) to the excited state (LUMO), making it a top candidate for CO_2 photoreduction. At the same time, this approach paves the path for the bottom-up fabrication of carbon nitride nanosheets.

1. Introduction

Overuse of fossil fuels is causing an increasingly urgent energy crisis and endangering the environment [1–5]. To find alternatives, researchers are developing promising renewable energy sources, such as photovoltaic and photocatalytic devices, that can be used to convert a certain amount of solar energy into sustainable energy sources [6–9]. The emission of greenhouse gases has hit a record level in the last century. Carbon dioxide (CO_2) is the primary concern for the global atmosphere due to fossil fuel combustion in the previous decades [10–12]. To date, several valuable technologies have been explored to convert CO_2 into renewable fuels as a potential solution to this inescapable global issue [13–15]. Among these, inspired by natural photosynthesis, using a semiconductor mediator to transform solar energy into chemical energy, by consuming CO_2 and water, is the most promising one [16,17]. A wide range of semiconductors have been studied so far for this purpose. However, most of these semiconductors have lost their value for being active only under UV light, made of costly precious metals, or photocatalytically not stable in the long run [18–20]. Therefore, it is critical to highlight metal-free semiconductors with extended consistency, low cost, easy availability, active under visible light, and rapid activation response. Carbon nitride (CN) is a metal-free semiconductor made up of carbon and nitrogen with an intrinsic bandgap of 2.7 eV. CN is highly durable, inexpensive, active under visible light, and needs simple procedures to alter its textural and electronic structure [21–24]. To date, techniques such as doping, nanostructuring, coupling, and sensitization have been used to increase the photocatalytic efficiency of CN [25–27]. Furthermore, several metals, non-metals, and monomers have been integrated into the primary structure of CN to improve its photocatalytic behavior and selectivity [28–31]. Recently, it has shown excellent performance in the photoreduction in CO_2 due to its wide surface area, which allows charge carriers to be transported to active sites [32–34]. However, the photocatalytic activity of copolymerized CN for CO_2 reduction is still insufficient. Therefore, several researchers have used a cobalt (Co) co-catalyst to make it much more active for CO_2 reduction. Incorporating Co into these photochemical systems makes the catalytic oxidation and reduction mechanism easy by promoting the charge carrier isolation and transportation [35–38]. Moreover, it is essential to fabricate CN nanosheets with wider visible light sensitivity. Due to the outstanding visible light absorption capabilities, porphyrins have been frequently employed as a photosensitizer in photochemical systems. So far, in porphyrin-based heterojunction with CN, porphyrin connects with CN through feeble electrostatic forces such as π-π staking or hydrogen bonding [39,40]. However, due to the restricted absorption of porphyrin on the CN, it remains a difficult task to bring more extensive improvements in their photocatalytic properties [41,42]. Anyhow, the transmission of electrons between CN and porphyrin can be substantially increased by connecting them through covalent bonding, and thus their solar energy absorbance can be enhanced further [43,44].

In the present work, we implanted organic conjugated monomer TDP into the triazine structure of CN through covalent bonding to construct promising carbon nitride nanosheets (Scheme 1). Initially, via mechanical mixing, TDP, and urea were connected by hydrogen bonding to form supramolecular complexes before heating. Through thermal polymerization (150–300 °C), a urea-TDP solution was generated, where TDP in the molecular state was evenly dispersed in the solution [21]. Furthermore, at 234 °C, the melamine

was formed as a chemically activated intermediate, which subsequently undergoes copolymerization at around 390 °C with 2, 4-diamino-1, 3, 5-triazinyl cluster of TDP. Finally, via covalent bonding, the integration of TDP into the CN frame has been achieved when the temperature was increased to 550 °C. As a result of this effective modification, CO_2 reduction improved significantly, credited to increased visible light absorption and better charge separation and transportation.
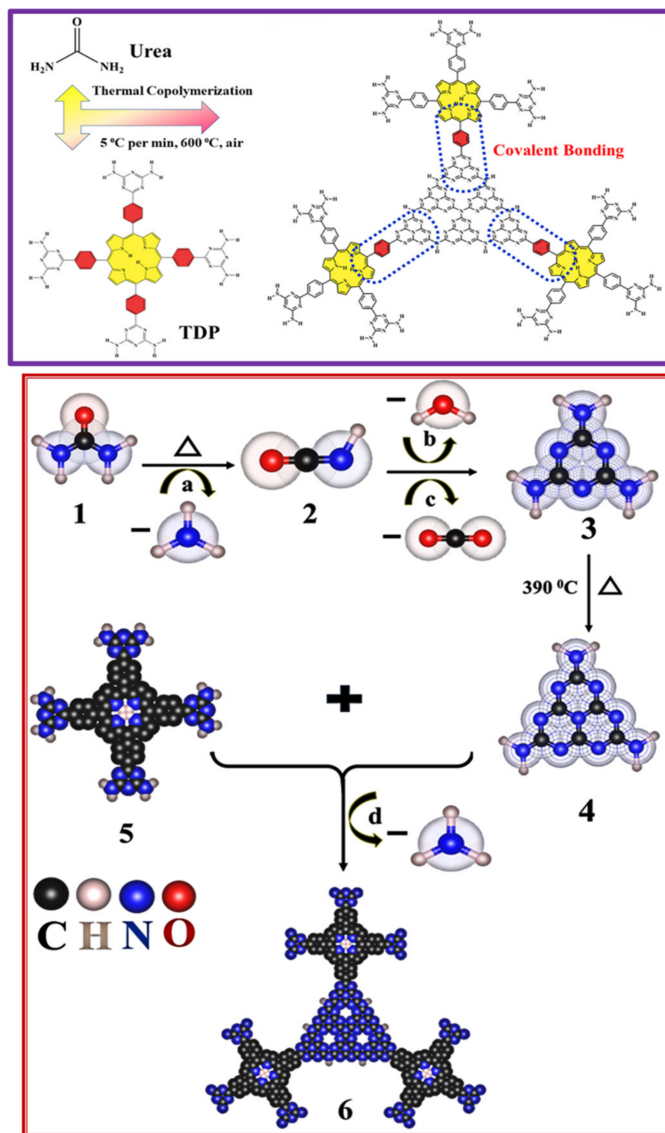
Scheme 1. Hydrogen bonded supramolecular complex assembly obtained between organic Urea-TDP. Conceivable reaction route of incorporation of TDP monomer into CN framework. Where 1: Urea, 2: Isocyanic acid, 3: 1, 3, 5-triazine-2,4,6-triamine, 4: Heptaazaphenalene-triamine, 5: TDP, and 6: CN-TDP. (a: Ammonia, b: H_2O, c: CO_2 and d: Ammonia).

2. Result and Discussion

The powder XRD of CN and modified CN-TDP$_x$, depicted in Figure 1a, shows that the structures are closely related. A well-resolved peak at 27.5° is indicating the (002) plane of graphitic, and another small peak at 12.7° is showing the in-plane repeated (100) units of heptazine. With the increasing volume of TDP in the structure of CN, it was discovered that the peak intensity at 27.5° was enhanced relative to pure CN. The incorporation of TDP in CN is the primary cause of change in the peak intensity. Fourier-transform infrared spectra (FT-IR) of the prepared samples are related to the heterocyclic structure

of CN, as presented in Figure 1b. The typical vibrational band peaks of heptazine can be found at 813 cm^{-1} and 1230 to 1630 cm^{-1}, respectively, confirming the presence of triazine subunits in all samples. The broad absorption peaks indexed at 2900 to 3100 cm^{-1} predict N-H vibration bands, which may be due to the uncondensed amine group at the surface and adsorbed water molecules [45,46]. All samples exhibit associated FT-IR vibrations, indicating structural integrity even after the copolymerization phase. Moreover, the BET phenomenon was utilized to determine the specific surface area of the as-prepared CN and CN-TDP$_{7.0}$ photocatalysts (Figure 1c). BET surface area for CN-TDP$_{7.0}$ after copolymerization is 179.27 m^2g^{-1}, compared to 65.43 m^2g^{-1} for a blank sample of CN under the same conditions. Nitrogen adsorption and desorption isotherms were used to analyze pore size diameter, as shown in Figure 1d. The pore size distribution reveals a greater pore size for CN-TDP$_{7.0}$ over CN due to the compact nanosheet. It was found that the increased surface area and pore size diameters for copolymerized samples resulted in better photocatalytic CO_2 reduction. Thermal stability of superior sample CN-TDP$_{7.0}$ was demonstrated through thermogravimetric analysis (TGA) as shown in Figure S3. As explained in the experimental portion, that samples were synthesized at constant temperature of 600 °C under static air has been identified from TGA curve. Secondly, the thermal degradation of sample has been observed around 650 °C may be related to the crosslinking in the sample.

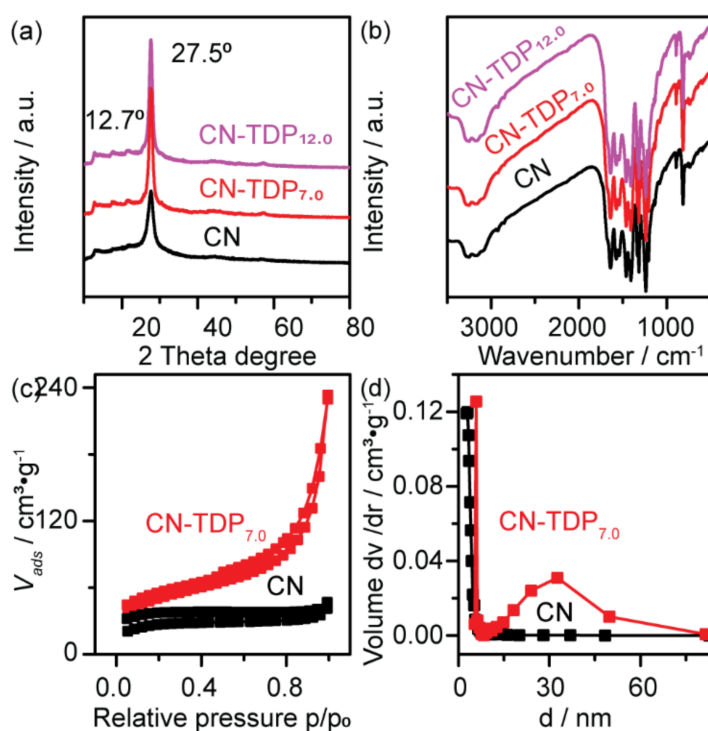**Figure 1.** (**a**) PXRD (**b**) FT-IR, (**c**) Nitrogen adsorption-desorption, (**d**) corresponding pore size distribution for CN and modified CN-TDP$_{7.0}$.

In Figure 2a, the SEM measurements show that the CN nanosheets are closely packed. However, the morphology did not sustain after adding TDP monomer (change from nanosheets to irregular rough surface nanoparticles). At the same time, Figure 2b shows magnified irregular nanoparticles with an average diameter of 70–100 nm for CN-TDP$_x$. Asymmetrical, thick, and compressed nanosheets can be seen in Figure 2c for CN, while suppressed surface morphology was observed for CN-TDP$_{7.0}$ with transparent, smooth, tinny, and much-reduced size, as well as silk-like nanostructures for CN-TDP$_{7.0}$ were found (Figure 2d).
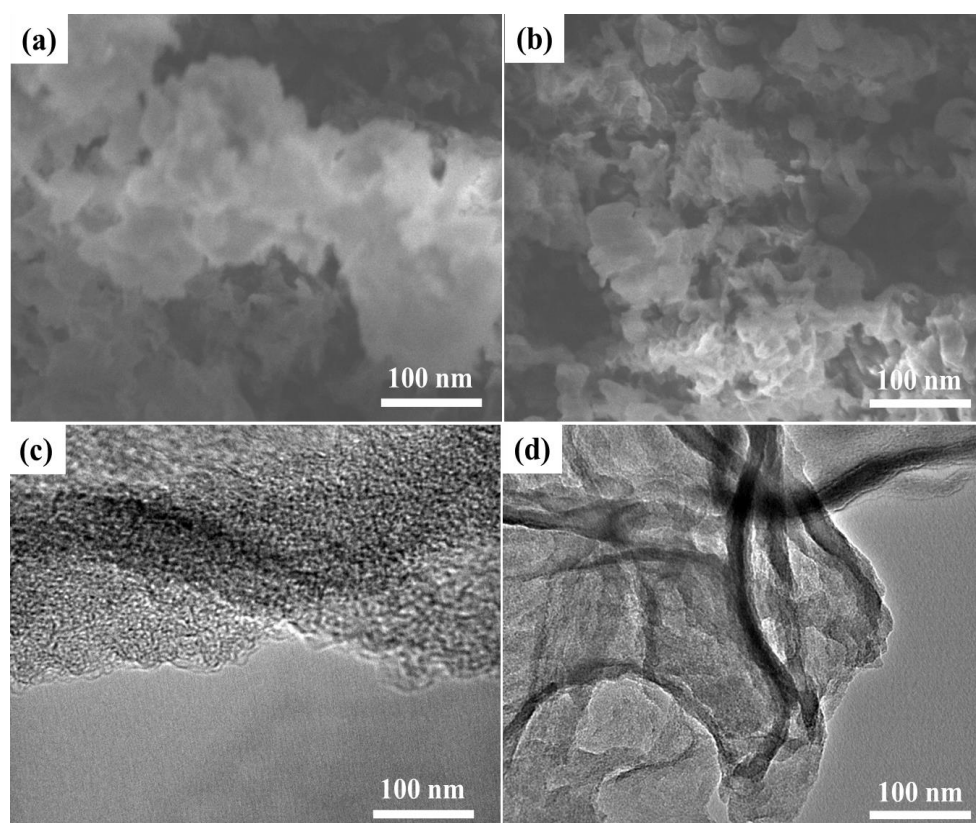
Figure 2. (**a**) SEM image for CN and (**b**) for CN-TDP$_{7.0}$. (**c**) TEM image for CN and (**d**) for CN-TDP$_{7.0}$ samples.

The photoluminescence (PL) signals moved from shorter to extended wavelength as the dopant (TDP) concentration was increased, as shown in Figure 3a. The result indicates that the CN-TDP nanosheets displayed fluorescence quenching, suggesting a lower recombination rate for the photogenerated charges and enhanced separation efficiency [47]. Such a quenching might be due to the synergistic effect of the CN-TDP nanosheet's decreased thickness and the creation of molecular heterojunction between TDP and CN components, forcing the charge carriers to move to the surface. It can be seen from the UV-visible spectrum in Figure 3b that the optical edges of the CN-TDP$_{7.0}$ material clearly experienced a shift to 430 nm from 495 nm for CN. The thickness and smaller size of the particles might be the main reason for such a shift that results in the quantum confinement effect. With the integration of varying amounts of TDP, the absorption range spread up to 500 nm, owing to the superior optical absorption performance for the TDP [41,48]. Further, optical band gaps were found to be shifted from 2.95 for CN to 2.71–2.54 eV for varying the amount of TDP. The induction of conjugated TDP into the skeleton of CN significantly reduces the p-electron delocalization within the conjugated system of the CN by generating photogenerated electrons-hole pairs, resulting in a simple decline in the related band gap as described in the DRS section. Furthermore, the electron paramagnetic resonance (EPR) spectrum was utilized to determine the origin of electronic band assembly for both CN and TDP integrated CNs, as shown in Figure 3c. Compared to CN, the strength of the Lorentzian line attributed, to the carbon atom, unpaired electrons in CN-TDP$_{7.0}$ (g = 2.003) was clearly increased [49,50]. It was observed that, once TDP was embedded in the skeleton of the CN at room temperature (RT) in the dark condition, the productivity of excited electrons separation and the thickness of the electron signals increased considerably. The elemental analysis was determined for each element within the samples (Figure 3d). The superior sample CN-TDP$_{7.0}$ manifests a significant elemental composition and a high value of C/N ratio due to the copolymerization process (Table S1).

More crucially, the solid-state ^{13}C NMR technique was utilized to analyze the quantity of carbon-containing compounds involved in CN after molecular doping. The results showed that the spectrum acquired for Pure CN and CN-TDP$_{7.0}$ materials were essentially identical, although a new additional peak was discovered for CN-TDP$_{7.0}$ at 20.26 ppm, as shown in Figure S2. This indicates that a novel species, such as carbon contents, was created by the copolymerization interaction of TDP monomer with CN.
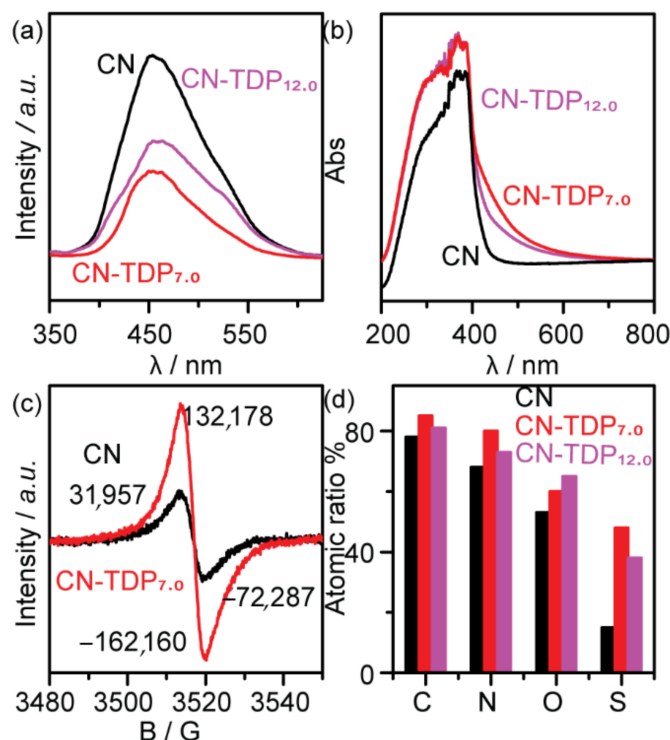

Figure 3. (**a**) photoluminescence spectra, (**b**) UV-Visible DRS, (**c**) EPR spectra in the dark at RT for CN and CN-TDP$_{7.0}$ samples. (**d**) Elemental analysis and C/N molar ratio for all samples under visible light ($\lambda > 420$ nm).

X-ray photoelectron spectroscopy (XPS) was utilized to examine the elemental chemical arrangement and composition of the samples. The results show that both samples, CN and CN-TDP$_{7.0}$, mostly have C, N, with a minor quantity of O element. The XPS spectra of C 1s show two major peaks at 287.8, 284.5 eV for CN and 288.4, 285.3 eV for CN-TDP$_{7.0}$ can be assigned to carbon coordination to N (N-C=N) and at 284.6 eV due to sp^2 trigonal planar hybridized carbon in the s-triazine ring, (Figure 4a,b). Similarly, the XPS spectrum of N 1s (Figure 4c–d) shows peaks at 398.2, 400.2, 404.4 eV for CN and 399.0, 400.4, 404.9 eV for CN-TDP$_{7.0}$ can be due to sp^2-hybridized N of the triazine system (C-N=N) bonds, terminal N-(C)^3 clusters and amino groups, respectively. In Figure S1†, the wide XPS spectrum and O 1s XPS spectra can be seen for CN and CN-TDP$_{7.0}$ samples.

2.1. Photocatalytic Property of CO$_2$ Reduction

CN and CN-TDP$_{7.0}$ were utilized for the photocatalytic reduction in CO$_2$ under visible light irradiation to convert CO$_2$ into CO and [O] products. Reactions were run at 30 °C and 1 atm in an aqueous medium containing acetonitrile (MeCN). Due to its high solubility in acetonitrile than water at standard atmospheric pressure, acetonitrile was used as the primary solvent. The reaction medium was consist of Co(bpy)$_3$$^{2+}$ as a photosensitizer and co-catalyst, triethanolamine (TEOA) as a sacrificial agent, and CO$_2$. Through an oxidative dehydrogenation process with the help of TEOA, releases hydrogen H$_2$, which combines with [O] to form H$_2$O. Under the same conditions, 4 h long controlled experiments, involving the reduction of CO$_2$ into CO and H$_2$, were carried out to test the practicality

of the CN-TDP$_{7.0}$ as a photocatalyst. Figure 5a shows the evolution of CO (64.71 mol) and H$_2$ (11.29 mol) product gases after photooxidation of CO$_2$ with the help of photocatalyst under solar light, emphasizing the improved photocatalytic activity for CO$_2$. As a result, the device continues to deliver high selectivity of CO, with a maximum yield in the early hours compared to H$_2$, but as the reaction time increases, the yield steadily decreases. The degradation of the [Ru(bpy)$_3$]Cl$_2$ photosensitizer is the fundamental cause of its decreased photocatalytic activity after a prolonged reaction [51]. Furthermore, long-term stability tests were applied to determine the stability parameter of the CN-TDP$_{7.0}$. To test, the used CN-TDP$_{7.0}$ catalyst was cleaned, retrieved, and spread into a Schlenk bottle holding a fresh sacrificial agent and photosensitizer under similar circumstances. Five recycling tests were carried out concurrently to test the reliability of the photocatalyst for CO$_2$ reduction, with the catalyst being washed and reused after each step. As seen in Figure 5b, after individual series, the recycled photocatalyst shows a minor decline in CO growth, meaning that it is the most stable catalyst for CO evolution. Likewise, to examine whether the excitation of TDP$_{7.0}$ induced CN depends on the incident light wavelength for the photocatalytic production of CO and H$_2$, supervised experiments have been carried out under the same conditions by adjusting the cut-off filter, as shown in Figure 5c. The yield of CO is almost equal to the optical absorption spectrum of CN-TDP$_{7.0}$, as seen in the systematic figure. The sum of H$_2$ and CO declines as the wavelength increases. This finding supports the theory that using the copolymerization principle with a CN semiconductor improves CO$_2$ photoreduction under artificial photosynthesis by improving charge separation and increasing the wavelength intensity to 510 nm. Under similar conditions, experiments were run by using different organic solvents, namely Dimethyl sulfoxide (DMSO), N, N-dimethylformamide (DMF), tetrahydrofuran (THF), and trichloromethane (TCM) for CO$_2$ reduction, as shown in Figure 5d. The figure shows certain solvents that are good for CO$_2$ reduction since they contain a lot of nitrogen and oxygen species, which can easily dissolve CO$_2$ during the reaction and increase the amount of CO in different media, particularly MeCN and THF solvents.
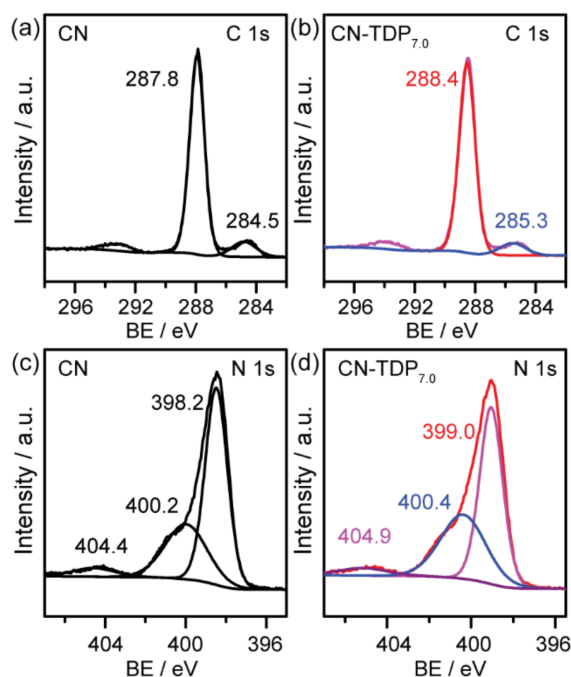

Figure 4. High-resolution XPS spectra of CN and CN-TDP$_{7.0}$. (**a–b**) for C 1s and (**c–d**) for N 1s, respectively.

Similarly, under the same condition, the reaction system was utilized using different amounts of TDP and precursors of CN along with pure samples as a comparison (Figure 6a).

Results demonstrate that CN, synthesized from urea and its copolymerized CN-TDP$_{7.0}$, is the most favorable sample for enhanced evolution of CO from the CO$_2$ reduction reaction system. More specifically, the reaction system was investigated to determine the effect of temperature on the evolution of CO from CO$_2$ photoreduction. As a result, the reaction system was tested at different temperatures (10–60 °C), as shown in Figure 6b. The volume of CO produced increases to its maximum value of 43.32 mol h^{-1} as the temperature rises from 20 °C to 30 °C, with a CO selectivity of 88.2 % (inset Figure 5d). As the reaction temperature increases above 30 °C, the photocatalytic efficiency of the catalyst declines, implying that the photocatalytic operation is maximum at the optimal temperature of 30 °C. Several experiments have been conducted under similar conditions to establish that CO$_2$ photoreduction initiated by CN-TDP$_{7.0}$ catalyst, when performed without the inclusion of the primary catalyst, results in no CO or H$_2$ evolution, highlighting the importance of CN-TDP$_{7.0}$ in the photocatalysis of CO$_2$ reduction. In order to determine whether the reaction mechanism is photocatalytic, the reaction was carried out in the dark. Again no observation of CO or H$_2$ implies that the system only stabilizes and maintains photocatalytic activity under the light. Regulated trials have also been carried out in the absence of photosensitizers such as [Ru(bby)$_3$] and TEOA. However, the investigation shows a weak production of CO and H$_2$ without Cl$_2$ and CoCl$_2$ (Table S2). Similarly, the reaction mechanism was tested by exchanging N$_2$ and Ar gas instead of CO$_2$ and using various sacrificial agents such as lactic acid and formic acid instead of triethanolamine, demonstrating the inadequate identification of the resultant CO and H$_2$. The data show that the reaction systems are photocatalytically inactive, and these factors are critical in activating and progressing the reaction mechanism toward greater photocatalytic CO$_2$ reduction.
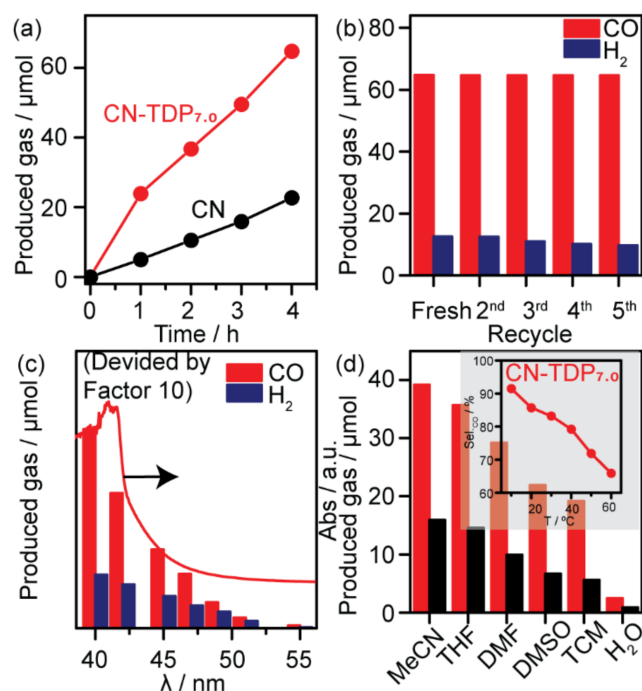

Figure 5. (**a**) Time function CO$_2$ reduction reaction. (**b**) Stability experiments of CN-TDP$_{7.0}$ photocatalyst. (**c**) Different wavelength experiments. (**d**) Different solvent experiments by using as-synthesized samples under visible light.

The charge isolation, migration, and generation on the interface of concern samples are examined by using photo-electrochemical analyses of the as-prepared samples. Figure 7a shows the photocurrent of parental CN and CN-TDP$_{7.0}$ photocatalyst, clearly demonstrating that the photocurrent intensity of CN increases abruptly after doping with TDP, presumably due to the efficient photogenerated charges, decrease in electron-hole pairs oxo-reductive potential, and enhancement of optical absorption on the TDP copolymer

interface. The rapid charge recombination of CN-TDP$_{7.0}$ increases the surface area and optical absorbance. Thus these two candidates are the key factors for significantly improving photocatalytic activity, especially in heterogeneous photocatalytic CO_2 reduction reactions. Charge recombination directly relates to surface area and optical absorbance, so a photocatalyst would raise the surface area, widen the optical absorbance, and decrease the recombination rate. A much lower semicircular Nyquist plot was observed for CN-TDP$_{7.0}$ than CN in the dark, demonstrating that the combination of TDP monomer in the framework of CN increased its electronic conductivity and thereby improved its charge isolation, as shown in Figure 7b.
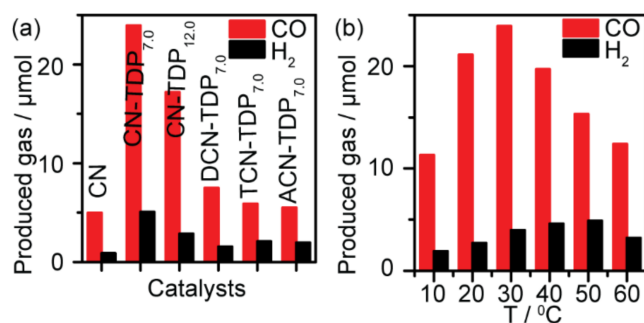

Figure 6. (**a**) CO_2 reduction reaction by using different catalysts for comparison. (**b**) Different organic solvent CO_2 reduction reactions at given conditions under visible light.
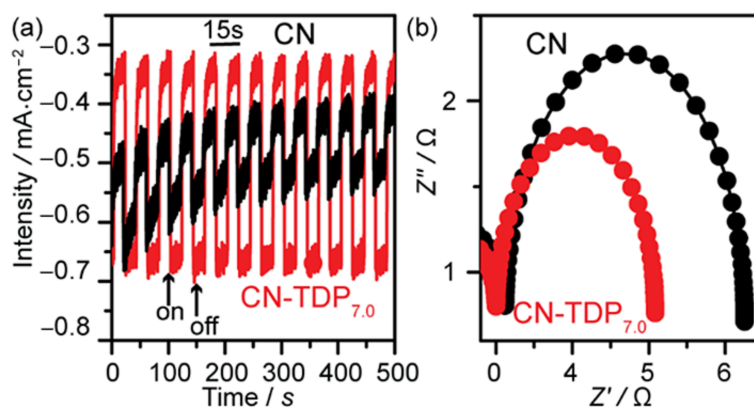

Figure 7. (**a**) The photocurrent response of CN-TDP$_{7.0}$ as compared with CN, (**b**) the electrochemical impedance spectroscopy (EIS) Nyquist graph in dark condition for pure CN and modified CN-TDP$_{7.0}$.

2.2. Mechanism of CO_2 Reduction Reaction

The possible photocatalytic mechanism under visible light for CO_2 reduction by CN-TDP$_{7.0}$ is depicted in Figure 8. Initially, the excitation of CN-TDP$_{7.0}$ promotes charge carrier production, separation, and their interfacial transmission. An occurrence of an electron intermediary with a co-catalyst suggesting that the transmission speeds up to the surface. As a result, high-energy electrons and holes were created. Later the cyclic translation of CO_2 and an oxidable of organic moiety take place. After the oxidative dehydrogenation of TEOA, the stimulated CO_2 was photocatalytically divided into CO and [O], with H_2 as a co-product. The overall reaction is:

$$CO_2 + 2H^+ + 2e \rightarrow CO + H_2O$$

The organic substrate TEOA still provides both protons and electrons. In this case, water might theoretically serve as a long-term supply of electrons and protons for this cross photochemical system.
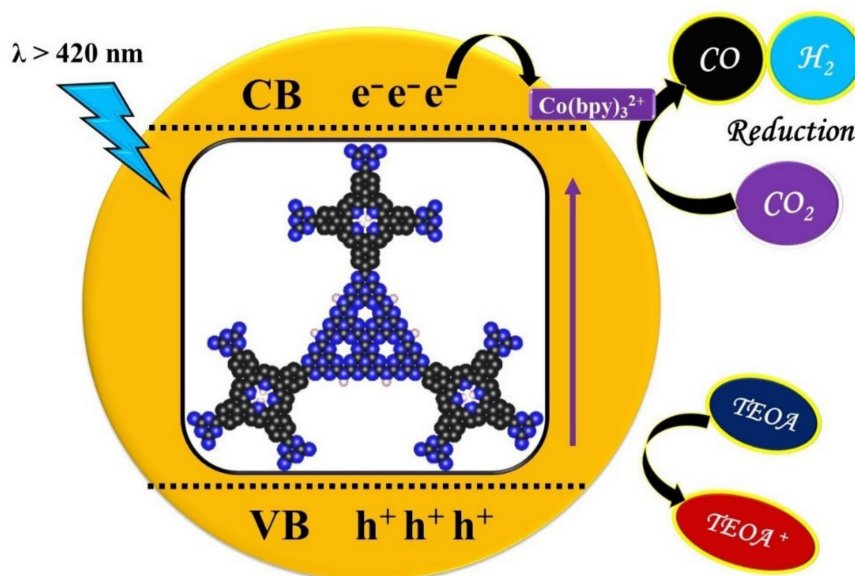
Figure 8. Under visible light irradiation, cobalt redox catalysis and CN-TDP$_{7.0}$ photocatalysis work together to activate and reduce CO_2 to CO.

3. Experimental

Preparation of Pure CN and Modified CN-TDP

The CN samples were prepared by using urea as a major precursor. Typically, 15 g of urea was heated directly at 600 °C (5 °C min^{-1}) in an air furnace for about 2 h. To make TDP modified CN (CH-TDP$_x$), a varied quantity of TDP (x = 7.0, 12.0 mg) was mixed with a fixed amount of urea (15 g) in 15 mL of distilled water and kept in a glycerol-based oil bath at 90 °C with constant stirring for a whole day and night until the water was entirely evaporated. After that, the solid wastes were placed in a crucible and calcined for 2 h in an air furnace at 600 °C (5 °C min^{-1}). The as-prepared samples were grounded into power and utilized for subsequent procedures and characterization after cooling to room temperature.

4. Conclusions

Finally, the bottom-up production of porphyrin-modified CN was carried out through covalent bonding for boosted CO_2 reduction. The integration of TDP into the triazine skeleton of CN significantly improves and promotes CO_2 photoreduction into CO materials. Such integration facilitates the current, surface, and structural properties of CN. Speeding up the electron charge transmission reduces the electron-hole recombination and enhances the optical absorption properties. Hence, proving this photocatalyst as one of the best candidates for heterogeneous catalysis. Our best sample (CN-TDP$_{7.0}$) achieved fantastic CO_2 photoconversion, with a 15-fold-enhanced catalytic efficiency, compared to the blank CN sample. It is fair to assume that the widespread use of the thermal polymerization technique improves the catalytic efficiency of CN for CO_2 photoreduction into CO when exposed to visible light.

References

1. Ahmed, G.; Hanif, M.; Mahmood, K.; Yao, R.; Ning, H.; Jiao, D.; Wu, M.; Khan, J.; Liu, Z. Lattice defects of ZnO and hybrids with GO: Characterization, EPR and optoelectronic properties. *AIP Adv.* **2018**, *8*, 025218. [CrossRef]
2. Khan, A.; Nair, V.; Colmenares, J.C.; Gläser, R. Lignin-based composite materials for photocatalysis and photovoltaics. *Top. Curr. Chem.* **2018**, *376*, 1–31. [CrossRef]
3. Khan, J.; Gu, J.; He, S.; Li, X.; Ahmed, G.; Liu, Z.; Akhtar, M.N.; Mai, W.; Wu, M. Rational design of a tripartite-layered TiO_2 photoelectrode: A candidate for enhanced power conversion efficiency in dye sensitized solar cells. *Nanoscale* **2017**, *9*, 9913–9920. [CrossRef]
4. Khan, J.; Gu, J.; Meng, Y.; Chai, Z.; He, S.; Wu, Q.; Tong, S.; Ahmed, G.; Mai, W.; Wu, M. Anatase TiO_2 single crystal hollow nanoparticles: Their facile synthesis and high-performance in dye-sensitized solar cells. *CrystEngComm* **2017**, *19*, 325–334. [CrossRef]
5. Hayat, A.; Raziq, F.; Khan, M.; Ullah, I.; Khan, W.U.; Khan, J.; Ahmad, A. Visible-light enhanced photocatalytic performance of polypyrrole/g-C_3N_4 composites for water splitting to evolve H_2 and pollutants degradation. *J. Photochem. Photobiol. A Chem.* **2019**, *379*, 88–98. [CrossRef]
6. Gu, J.; Khan, J.; Chai, Z.; Yuan, Y.; Yu, X.; Liu, P.; Wu, M.; Mai, W. Rational design of anatase TiO_2 architecture with hierarchical nanotubes and hollow microspheres for high-performance dye-sensitized solar cells. *J. Power Sources* **2016**, *303*, 57–64. [CrossRef]
7. Khan, J.; Rahman, N.U.; Khan, W.U.; Hayat, A.; Yang, Z.; Ahmed, G.; Akhtar, M.N.; Tong, S.; Chi, Z.; Wu, M. Multi-dimensional anatase TiO_2 materials: Synthesis and their application as efficient charge transporter in perovskite solar cells. *Sol. Energy* **2019**, *184*, 323–330. [CrossRef]
8. Khan, J.; Rahman, N.U.; Khan, W.U.; Wang, Y.; Fu, S.; Ahmed, G.; Akhtar, M.N.; Wu, M. Hollow 3D TiO_2 sub-microspheres as an electron transporting layer for highly efficient perovskite solar cells. *Mater. Today Energy* **2021**, *19*, 100614. [CrossRef]
9. Li, S.H.; Liu, S.; Colmenares, J.C.; Xu, Y.J. A sustainable approach for lignin valorization by heterogeneous photocatalysis. *Green Chem.* **2016**, *18*, 594–607. [CrossRef]
10. Ahmed, G.; Raziq, F.; Hanif, M.; Khan, J.; Munawar, K.S.; Wu, M.; Cao, X.; Liu, Z. Oxygen-Cluster-Modified Anatase with Graphene Leads to Efficient and Recyclable Photo-Catalytic Conversion of CO_2 to CH_4 Supported by the Positron Annihilation Study. *Sci. Rep.* **2019**, *9*, 1–8. [CrossRef]
11. Barrio, J.; Volokh, M.; Shalom, M. Polymeric carbon nitrides and related metal-free materials for energy and environmental applications. *J. Mater. Chem. A* **2020**, *8*, 11075–11116. [CrossRef]
12. Hayat, A.; Khan, J.; Rahman, M.U.; Mane, S.B.; Khan, W.U.; Sohail, M.; Rahman, N.U.; Shaishta, N.; Chi, Z.; Wu, M. Synthesis and optimization of the trimesic acid modified polymeric carbon nitride for enhanced photocatalytic reduction of CO_2. *J. Colloid Interface Sci.* **2019**, *548*, 197–205. [CrossRef]
13. Lin, L.; Hou, C.; Zhang, X.; Wang, Y.; Chen, Y.; He, T. Highly efficient visible-light driven photocatalytic reduction of CO_2 over g-C_3N_4 nanosheets/tetra (4-carboxyphenyl) porphyrin iron (III) chloride heterogeneous catalysts. *Appl. Catal. B Environ.* **2018**, *221*, 312–319. [CrossRef]
14. Le, S.; Jiang, T.; Zhao, Q.; Liu, X.; Li, Y.; Fang, B.; Gong, M. Cu-doped mesoporous graphitic carbon nitride for enhanced visible-light driven photocatalysis. *RSC Adv.* **2016**, *6*, 38811–38819. [CrossRef]
15. Li, K.; Zhang, W.D. Creating graphitic carbon nitride based donor-π–acceptor-π–donor structured catalysts for highly photocatalytic hydrogen evolution. *Small* **2018**, *14*, 1703599. [CrossRef] [PubMed]
16. Ong, W.J.; Tan, L.L.; Ng, Y.H.; Yong, S.T.; Chai, S.P. Graphitic carbon nitride (g-C_3N_4)-based photocatalysts for artificial photosynthesis and environmental remediation: Are we a step closer to achieving sustainability? *Chem. Rev.* **2016**, *116*, 7159–7329. [CrossRef]
17. Qin, J.; Wang, S.; Ren, H.; Hou, Y.; Wang, X. Photocatalytic reduction of CO_2 by graphitic carbon nitride polymers derived from urea and barbituric acid. *Appl. Catal. B Environ.* **2015**, *179*, 1–8. [CrossRef]
18. Hayat, A.; Rahman, M.U.; Khan, I.; Khan, J.; Sohail, M.; Yasmeen, H.; Liu, S.-Y.; Qi, K.; Lv, W. Conjugated electron donor–acceptor hybrid polymeric carbon nitride as a photocatalyst for CO_2 reduction. *Molecules* **2019**, *24*, 1779. [CrossRef]
19. Hayat, A.; Raziq, F.; Khan, M.; Khan, J.; Mane, S.K.B.; Ahmad, A.; Rahman, M.U.; Khan, W.U. Fusion of conjugated bicyclic co-polymer within polymeric carbon nitride for high photocatalytic performance. *J. Colloid Interface Sci.* **2019**, *554*, 627–639. [CrossRef]

20. Rao, H.; Lim, C.H.; Bonin, J.; Miyake, G.M.; Robert, M. Visible-light-driven conversion of CO_2 to CH_4 with an organic sensitizer and an iron porphyrin catalyst. *J. Am. Chem. Soc.* **2018**, *140*, 17830–17834. [CrossRef]

21. Qu, D.; Liu, J.; Miao, X.; Han, M.; Zhang, H.; Cui, Z.; Sun, S.; Kang, Z.; Fan, H.; Sun, Z. Peering into water splitting mechanism of g-C_3N_4-carbon dots metal-free photocatalyst. *Appl. Catal. B Environ.* **2018**, *227*, 418–424. [CrossRef]

22. Zhang, G.; Li, G.; Heil, T.; Zafeiratos, S.; Lai, F.; Savateev, A.; Antonietti, M.; Wang, X. Tailoring the grain boundary chemistry of polymeric carbon nitride for enhanced solar hydrogen production and CO_2 reduction. *Angew. Chem. Int. Ed.* **2019**, *58*, 3433–3437. [CrossRef] [PubMed]

23. Huang, P.; Huang, J.; Pantovich, S.A.; Carl, A.D.; Fenton, T.G.; Caputo, C.A.; Grimm, R.L.; Frenkel, A.I.; Li, G. Selective CO_2 reduction catalyzed by single cobalt sites on carbon nitride under visible-light irradiation. *J. Am. Chem. Soc.* **2018**, *140*, 16042–16047. [CrossRef]

24. Hayat, A.; Shaishta, N.; Mane, S.K.B.; Khan, J.; Hayat, A. Rational Ionothermal copolymerization of TCNQ with PCN semiconductor for enhanced Photocatalytic full water splitting. *ACS Appl. Mater. Interfaces* **2019**, *11*, 46756–46766. [CrossRef]

25. Chen, H.; Wang, L. Nanostructure sensitization of transition metal oxides for visible-light photocatalysis. *Beilstein J. Nanotechnol.* **2014**, *5*, 696–710. [CrossRef]

26. Quan, H.; Gao, Y.; Wang, W. Tungsten oxide-based visible light-driven photocatalysts: Crystal and electronic structures and strategies for photocatalytic efficiency enhancement. *Inorg. Chem. Front.* **2020**, *7*, 817–838. [CrossRef]

27. Mohammadzadeh, A.; Khoshghadam-Pireyousefan, M.; Shokrianfard-Ravasjan, B.; Azadbeh, M.; Rashedi, H.; Dibazar, M.; Mostafaei, A. Synergetic photocatalytic effect of high purity ZnO pod shaped nanostructures with H_2O_2 on methylene blue dye degradation. *J. Alloy. Compd.* **2020**, *845*, 156333. [CrossRef]

28. Lu, X.; Xu, K.; Chen, P.; Jia, K.; Liu, S.; Wu, C. Facile one step method realizing scalable production of gC_3N_4 nanosheets and study of their photocatalytic H_2 evolution activity. *J. Mater. Chem. A* **2014**, *2*, 18924–18928. [CrossRef]

29. Tang, M.; Ao, Y.; Wang, C.; Wang, P. Facile synthesis of dual Z-scheme g-C_3N_4/Ag_3PO_4/AgI composite photocatalysts with enhanced performance for the degradation of a typical neonicotinoid pesticide. *Appl. Catal. B Environ.* **2020**, *268*, 118395. [CrossRef]

30. Ullah, A.; Khan, J.; Sohail, M.; Hayat, A.; Zhao, T.K.; Ullah, B.; Khan, M.; Uddin, I.; Ullah, S.; Ullah, R. Fabrication of polymer carbon nitride with organic monomer for effective photocatalytic hydrogen evolution. *J. Photochem. Photobiol. A Chem.* **2020**, *401*, 112764. [CrossRef]

31. Wang, J.; Cao, S.; Yu, J. Nanocages of Polymeric Carbon Nitride from Low-Temperature Supramolecular Preorganization for Photocatalytic CO_2 Reduction. *Sol. RRL* **2020**, *4*, 1900469. [CrossRef]

32. Hayat, A.; Shaishta, N.; Mane, S.K.B.; Hayat, A.; Khan, J.; Rehman, A.U.; Li, T. Molecular engineering of polymeric carbon nitride based Donor-Acceptor conjugated copolymers for enhanced photocatalytic full water splitting. *J. Colloid Interface Sci.* **2020**, *560*, 743–754. [CrossRef]

33. Huang, T.; Pan, S.; Shi, L.; Yu, A.; Wang, X.; Fu, Y. Hollow porous prismatic graphitic carbon nitride with nitrogen vacancies and oxygen doping: A high-performance visible light-driven catalyst for nitrogen fixation. *Nanoscale* **2020**, *12*, 1833–1841. [CrossRef]

34. Hou, P.; Song, W.; Wang, X.; Hu, Z.; Kang, P. Well-Defined Single-Atom Cobalt Catalyst for Electrocatalytic Flue Gas CO_2 Reduction. *Small* **2020**, *16*, 2001896. [CrossRef] [PubMed]

35. Ma, B.; Chen, G.; Fave, C.; Chen, L.; Kuriki, R.; Maeda, K.; Ishitani, O.; Lau, T.-C.; Bonin, J.; Robert, M. Efficient visible-light-driven CO_2 reduction by a cobalt molecular catalyst covalently linked to mesoporous carbon nitride. *J. Am. Chem. Soc.* **2020**, *142*, 6188–6195. [CrossRef]

36. Pei, G.X.; Dzade, N.Y.; Zhang, Y.; Hofmann, J.P.; De Leeuw, N.H.; Weckhuysen, B.M. Identification of photoexcited electron relaxation in a cobalt phosphide modified carbon nitride photocatalyst. *ChemPhotoChem* **2021**, *5*, 330–334. [CrossRef]

37. Zhang, N.; Wang, L.; Wang, H.; Cao, R.; Wang, J.; Bai, F.; Fan, H. Self-assembled one-dimensional porphyrin nanostructures with enhanced photocatalytic hydrogen generation. *Nano Lett.* **2018**, *18*, 560–566. [CrossRef] [PubMed]

38. Zhao, C.; Chen, Z.; Shi, R.; Yang, X.; Zhang, T. Recent Advances in Conjugated Polymers for Visible-Light-Driven Water Splitting. *Adv. Mater.* **2020**, *32*, 1907296. [CrossRef]

39. Wu, K.; Chen, X.; Liu, S.; Pan, Y.; Cheong, W.-C.; Zhu, W.; Cao, X.; Shen, R.; Chen, W.; Luo, J. Porphyrin-like Fe-N_4 sites with sulfur adjustment on hierarchical porous carbon for different rate-determining steps in oxygen reduction reaction. *Nano Res.* **2018**, *11*, 6260–6269. [CrossRef]

40. Zhao, G.; Pang, H.; Liu, G.; Li, P.; Liu, H.; Zhang, H.; Shi, L.; Ye, J. Co-porphyrin/carbon nitride hybrids for improved photocatalytic CO_2 reduction under visible light. *Appl. Catal. B Environ.* **2017**, *200*, 141–149. [CrossRef]

41. Tian, S.; Chen, S.; Ren, X.; Hu, Y.; Hu, H.; Sun, J.; Bai, F. An efficient visible-light photocatalyst for CO_2 reduction fabricated by cobalt porphyrin and graphitic carbon nitride via covalent bonding. *Nano Res.* **2020**, *13*, 2665–2672. [CrossRef]

42. Chaubey, S.; Singh, C.; Singh, P.; Kumar, A.; Pande, P.P.; Baeg, J.-O.; Dwivedi, D.K.; Yadav, R.K. Efficient photocatalytic synthesis of l-glutamate using a self-assembled carbon nitride/sulfur/porphyrin catalyst. *Environ. Chem. Lett.* **2020**, *18*, 1389–1395. [CrossRef]

43. Castro-Hermosa, S.; Wouk, L.; Bicalho, I.S.; de Queiroz Corrêa, L.; de Jong, B.; Cinà, L.; Brown, T.M.; Bagnis, D. Efficient fully blade-coated perovskite solar cells in air with nanometer-thick bathocuproine buffer layer. *Nano Res.* **2021**, *14*, 1034–1042. [CrossRef]

44. Li, H.J.W.; Zhou, H.; Chen, K.; Liu, K.; Li, S.; Jiang, K.; Zhang, W.; Xie, Y.; Cao, Z.; Li, H. Metallic MoO_2-Modified Graphitic Carbon Nitride Boosting Photocatalytic CO_2 Reduction via Schottky Junction. *Sol. RRL* **2020**, *4*, 1900416. [CrossRef]

45. Hayat, A.; Taha, T.A.; Alenad, A.M.; Ullah, I.; Shah, S.; Uddin, I.; Ullah, I.; Hayat, A.; Khan, W.U. A simplistic molecular agglomeration of carbon nitride for optimized photocatalytic performance. *Surf. Interfaces* **2021**, *25*, 101166. [CrossRef]

46. Liang, Z.; Zhuang, X.; Tang, Z.; Li, H.; Liu, L.; Kang, W. Soft-template induced synthesis of high-crystalline polymeric carbon nitride with boosted photocatalytic performance. *J. Mater. Chem. A* **2021**, *9*, 6805–6810. [CrossRef]

47. Hayat, A.; Chen, Z.; Luo, Z.; Fang, Y.; Wang, X. π-deficient pyridine ring-incorporated carbon nitride polymers for photocatalytic H_2 evolution and CO_2 fixation. *Res. Chem. Intermed.* **2021**, *47*, 15–27. [CrossRef]

48. Hayat, A.; Li, T. A facile supramolecular aggregation of trithiocyanuric acid with PCN for high photocatalytic hydrogen evolution from water splitting. *Int. J. Energy Res.* **2019**, *43*, 5479–5492. [CrossRef]

49. Hayat, A.; Alrowaili, Z.A.; Taha, T.A.; Khan, J.; Uddin, I.; Ali, T.; Raziq, F.; Ullah, I.; Hayat, A.; Palamanit, A.; et al. Organic heterostructure modified carbon nitride as apprehension for Quercetin Biosensor. *Synth. Met.* **2021**, *278*, 116813. [CrossRef]

50. Wisser, F.M.; Duguet, M.; Perrinet, Q.; Ghosh, A.C.; Alves-Favaro, M.; Mohr, Y.; Lorentz, C.; Quadrelli, E.A.; Palkovits, R.; Farrusseng, D.; et al. Molecular Porous Photosystems Tailored for Long-Term Photocatalytic CO_2 Reduction. *Angew. Chem. Int. Ed.* **2020**, *59*, 5116–5122. [CrossRef]

51. Bai, S.; Wang, Z.; Tan, L.; Waterhouse, G.I.; Zhao, Y.; Song, Y.F. 600 nm irradiation-induced efficient photocatalytic CO_2 reduction by ultrathin layered double hydroxide nanosheets. *Ind. Eng. Chem. Res.* **2020**, *59*, 5848–5857. [CrossRef]